



## Effect of the intercalated/exfoliated nanostructure on the phase transformations of smectic polyester/layered silicate hybrids: Reinforcement of the liquid-crystalline matrix

A. Martínez-Gómez<sup>a,1</sup>, E. Pérez<sup>b</sup>, C. Álvarez<sup>b,\*</sup>

<sup>a</sup>ETS de Ingenieros Industriales, Universidad Politécnica de Madrid, José Gutiérrez Abascal 2, 28006 Madrid, Spain

<sup>b</sup>Instituto de Ciencia y Tecnología de Polímeros, CSIC, Juan de la Cierva 3, 28006 Madrid, Spain

### ARTICLE INFO

#### Article history:

Received 17 November 2008

Received in revised form

22 January 2009

Accepted 23 January 2009

Available online 30 January 2009

#### Keywords:

Nanocomposite

Liquid-crystalline polymer

Smectic mesophases

### ABSTRACT

Smectic poly(triethylene glycol *p,p'*-bibenzoate) (PTEB)/clay hybrids were prepared by a solution blending method. Unmodified (cloisite<sup>®</sup>Na) and two organically modified (cloisite<sup>®</sup>10A and cloisite<sup>®</sup>15A) montmorillonites were used. The morphology of the hybrids was characterized by TEM and X-ray diffraction. It has been found that a conventional microcomposite is obtained from unmodified montmorillonite, while intercalated/exfoliated nanocomposites are produced from organoclays. Dynamic DSC and X-ray synchrotron studies show that the liquid-crystalline character of PTEB is preserved in the hybrids, and both the cooling phase sequence (isotropic melt–SmA–SmC) and smectic layer thickness of PTEB are practically unaffected by the presence of clay particles. However, the kinetics of evolution of PTEB to their different ordered states (liquid-crystalline and crystal) certainly depends on the morphology. Moreover, the effect of the clay morphology in the tensile reinforcement of the liquid-crystalline matrix is also analysed. The intercalated/exfoliated nanostructures show an increase about 200% in Young's modulus.

© 2009 Elsevier Ltd. All rights reserved.

### 1. Introduction

Among mesophase-forming polymers, aromatic polyesters constitute an important class of main-chain liquid-crystalline polymers (MLCPs). They present, however, some inconveniences such as a reduced solubility and very high transitions temperatures, thus making them difficult to process. The introduction of flexible aliphatic spacers between the mesogenic groups is a widely used method of reducing the isotropization temperatures of all aromatic, rod like polyesters [1]. Evidently, the mechanical performances of such thermotropic polymers are reduced when trying to increase their processability.

The interest in polymer layered silicate nanocomposites (PLSNs) is driven by the possibility of exceptional mechanical property enhancements at low filler levels [2]. The key to such performances rests in the ability to exfoliate and disperse individual high-aspect ratio silicate platelets within the polymer matrix. Among the

layered silicates, sodium montmorillonite (MMT) is particularly attractive as reinforcement for the polymer/clay hybrids because it is readily available in large amounts with relatively low cost. The hydrophilic nature of MMT surfaces prevents homogeneous dispersion throughout the hydrophobic polymer phase, so it is necessary to enhance the organophilicity of the layered silicate surface. Generally, this can be done through ion-exchange reactions that replace Na<sup>+</sup> cations with alkylammonium or alkylphosphonium cations. These organically modified montmorillonites (OMMT) can be readily exfoliated into nanolayers, leading to the formation of PLSNs.

Depending on the structure of dispersed clay layers in the polymer matrix, three main types of morphologies can be obtained: traditional microcomposites, intercalated and/or exfoliated nanocomposites. The intercalated structures result from diffusion of polymer chains into the clay galleries, leading to the formation of well-ordered multilayered structures. The exfoliated structures result when the individual silicate layers are well dispersed in a polymer matrix.

Few studies have been reported on the preparation of organoclay nanocomposites based on thermotropic liquid-crystalline polymers (TLCPs) [3–5]. It has been shown that TLCPs can give rise to intercalated OMMT aggregates which can lead to an improvement of

\* Corresponding author. Tel.: +34 91 5622900; fax: +34 91 5644853.

E-mail address: [crisrina.alvarez@ictp.csic.es](mailto:crisrina.alvarez@ictp.csic.es) (C. Álvarez).

<sup>1</sup> Present address: Instituto de Ciencia y Tecnología de Polímeros, CSIC, Juan de la Cierva 3, 28006 Madrid, Spain.

thermal stability and mechanical properties (stiffness and strength) of the matrix. The prospects for achieving a very high exfoliation degree of OMMT aggregates are low, due to the lack of compatibility between OMMT and TLCPs employed. Huang and Han [5] have shown that the design and synthesis of TLCPs with functional groups, which can have strong attractive interactions with OMMT, give rise to highly exfoliated nanocomposites without losing the liquid-crystalline character.

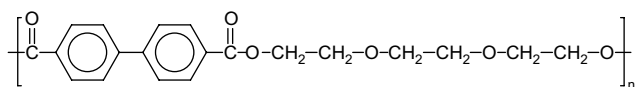
Our main goal is to prepare nanocomposites based on semi-flexible poly(bibenzoates), which are a kind of smectic polyester obtained by polycondensation of mesogenic bibenzoate group with a variety of diol spacers. Previous works [6–12] have shown that the nature of the spacer has strong effect on the liquid-crystalline behaviour and mechanical properties. We consider that these polyesters are adequate model systems for getting a better comprehension about the dispersion level effect (intercalated vs. exfoliated structures) on the liquid-crystalline character, besides analysing its effect on the reinforcement of the matrix.

In the present study, nanocomposites based on poly(triethylene glycol *p,p'*-bibenzoate) (PTEB) with natural and organophilic montmorillonites were prepared via intercalation of polymer from solution [13]. PTEB shows a SmC phase, which is rather stable although the transformation into a three dimensional crystal can be attained by annealing for long times at temperatures above the glass transition [14–16]. The main targets of this work have been: (1) to characterize the structure and dispersion of clay in the PTEB matrix of hybrids derived from different layered silicates, by combining X-ray diffraction and transmission electron microscopy; (2) to analyse how morphology attained affects the evolution of PTEB to their different ordered states (liquid-crystalline and crystal) and (3) to study the effect of this morphology in the reinforcement of the liquid-crystalline matrix.

## 2. Experimental

### 2.1. Materials

Poly(triethylene glycol *p,p'*-bibenzoate) (PTEB), was synthesized in our laboratory by transesterification of dimethyl 1,1'-biphenyl-4,4'-dicarboxylate (Aldrich) with triethylene glycol (Aldrich) using titanium (IV) isopropoxide as catalyst. The polymer was purified by precipitation from a chloroform solution using methanol. The chemical structure of PTEB:



was confirmed by NMR spectroscopy in deuterated chloroform. Further details concerning the synthesis and characterization of PTEB were given elsewhere [17].

Weight-average ( $M_w$ ) and number-average ( $M_n$ ) molecular weights and intrinsic viscosity of PTEB were determined by size-exclusion chromatography using a Water Alliance GPCV 2000, equipped with two detectors: the conventional refractive index concentration detector and a viscometer. The dual detection allows to achieve a universal calibration (obtained from measurements in different polystyrene standards, using chloroform as eluent at 35 °C), and to determine absolute molecular weight and viscosity values. The results obtained are  $M_w = 18,396$  and  $M_n = 9,063$ , and an intrinsic viscosity of  $0.335 \text{ dL g}^{-1}$ .

The layered silicates used in this study were a natural montmorillonite (Cloisite® Na, CNa) and two organically modified montmorillonites with different quaternary amine salts (Cloisite® 10A and Cloisite® 15A, C10A and C15A, respectively), supplied by

Southern Clay Products Inc. The chemical structure of quaternary amine and characteristics of clays [18] are presented in Table 1. To obtain hybrids with a silicate content around 2.4 wt%, an amount of OMMT close to 4 wt% was used.

### 2.2. Preparation of hybrid materials

Nanocomposites were prepared by using the solution blending method. Initially, the layered silicate is swollen in chloroform with the help of ultrasonic stirring for 2 h. Then, a predetermined amount of PTEB was dissolved in chloroform at room temperature and, subsequently, the suspended clay was added slowly into the polymer solution. The solution was kept under vigorous stirring at room temperature for 5 days. The final product was removed by precipitation in methanol and then it was dried under vacuum for 24 h at 60 °C.

Sheets specimens were obtained as films by compression moulding in a Collin press between hot plates at 130 °C, and then quenched down to room temperature with circulating water. The films were prepared between two chromed steel plates. A thin Teflon foil was placed between sample and each chromed steel plate to avoid problems of adhesion. The different hybrids are designated as follows: PTEB/ followed by the type of clay used (CNa, C10A or C15A).

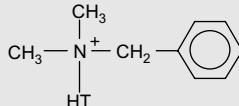
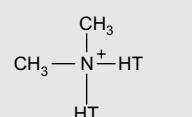
### 2.3. Techniques

Microtomed sections of the hybrids were examined by transmission electron microscopy (TEM) using a JEOL JEM-2000 FX electron microscope running at an accelerating voltage of 200 kV.

Wide-angle X-ray diffraction (WAXS) patterns were recorded in the reflection mode at room temperature by using a SEIFERT XRD 3000TT rotating anode X-ray generator with a Cu target and a Ni filter produced Cu K $\alpha$  radiation ( $\lambda = 0.154 \text{ nm}$ ). The diffraction scans were collected continuously, using a scanning rate of  $1^\circ \text{ min}^{-1}$  over a range of  $2\theta = 2\text{--}35^\circ$ .

Real-time X-ray diffraction experiments were performed in the soft-condensed matter beam-line A2 at HASYLAB with synchrotron light in DESY, Hamburg, Germany. A wavelength  $\lambda = 0.15 \text{ nm}$  was used. Simultaneous wide-angle (WAXS) and middle-angle (MAXS) profiles were acquired with a CCD detector, located at 17 cm from the sample, covering the  $2\theta$  range from 1.4 to 27.5 degrees. A semicrystalline PET standard sample was used for the WAXS calibration and a silver behenate for the MAXS one. Heating and cooling experiments were performed at  $8^\circ \text{ C min}^{-1}$ . Each frame was

**Table 1**  
Characteristics of the clays used in this study.

Clay type	Chemical structure of surfactant <sup>a</sup>	Concentration of OM meq. (100 g clay) <sup>-1</sup>	Surfactant content (%)	$d_{001}$ (nm)
CNa	None	None	0	1.17
C10A		125	39	1.92
C15A		125	43	3.15

<sup>a</sup> HT is hydrogenated tallow (~65% C18, ~30% C16, ~5% C14).

collected during 60 s and later corrected for background and primary beam intensity fluctuations during experiment.

Differential scanning calorimetry (DSC) measurements were performed under nitrogen atmosphere ( $20 \text{ ml min}^{-1}$ ) in a Perkin–Elmer DSC7 calorimeter, provided with a cooling system. About 6 mg of the sample was encapsulated in an aluminium pan. DSC experiments were carried out under non-isothermal and isothermal conditions. The glass transition temperature,  $T_g$ , was taken as the temperature where the specific heat increment is half of the total one at the transition, while the liquid-crystallization temperature,  $T_{LC}$ , and the isotropization temperature,  $T_i$ , were considered as the peak minimum or maximum. The enthalpy values were normalized to the PTEB mass in the hybrids.

Dynamic cooling–heating experiments were performed using a scanning rate of  $20 \text{ }^\circ\text{C min}^{-1}$ . The sample was first kept at  $135 \text{ }^\circ\text{C}$  for 2 min to remove the previous thermal history.

Two types of isothermal experiments were performed in order to study the liquid-crystallization and crystallization processes of PTEB. For the liquid-crystallization measurements, the samples were melted at  $135 \text{ }^\circ\text{C}$  for 2 min and, subsequently, were rapidly cooled to the chosen temperature in the range  $112\text{--}106 \text{ }^\circ\text{C}$ . The kinetics of the mesophase-crystal transformation was studied by the following procedure: the sample was fully melted at  $135 \text{ }^\circ\text{C}$  and quenched down to room temperature to obtain the mesophase. Then, the sample was kept in a furnace at  $85 \text{ }^\circ\text{C}$  for a certain annealing time,  $t_a$ , between 0 and 72 h. Finally, the DSC heating curve was registered at  $10 \text{ }^\circ\text{C min}^{-1}$  from  $85 \text{ }^\circ\text{C}$  to  $135 \text{ }^\circ\text{C}$ . The heat of fusion of the crystalline phase,  $\Delta H_m$ , was then determined as function of the annealing time.

Stress–strain curves were obtained from uniaxial tension experiments. Dumb-bell shaped specimens, with gauge dimensions 15 mm in length and 2 mm in width, were punched out from the liquid-crystalline films with a standardized die. The thickness of the specimens was in the range from 0.3 to 0.6 mm. Tensile testing was carried out using an MTS Synergie 200 machine calibrated according to standard procedures. All the samples were drawn at a crosshead speed of  $10 \text{ mm min}^{-1}$  and at room temperature. An average of at least 5 measurements for each sample is reported.

### 3. Results and discussion

#### 3.1. Morphology of PTEB/clay hybrids

Fig. 1 illustrates the wide-angle X-ray diffraction (WAXS) patterns at room temperature of pure PTEB and PTEB/clay hybrids in the region  $2\theta = 2\text{--}14^\circ$ , as well as the corresponding to the neat clays. The pattern of pure PTEB presents two small diffraction peaks at ca.  $5.1^\circ$  and  $10.2^\circ$  related to the first and second order of the smectic spacing, respectively. The patterns of clays exhibit a strong diffraction peak whose maximum position is in agreement with the mean interlayer spacing of the (001) plane,  $d_{001}$ , given in Table 1. In the case of C15A, the weak peak at  $7.2^\circ$  indicates that a small silicate population retains the laminar structure of the unmodified montmorillonite.

The X-ray patterns of PTEB/clay hybrids show the first and second order of the smectic reflection at  $5.1^\circ$  and  $10.2^\circ$ , respectively, indicating that the PTEB matrix retains its smectic structure. The presence of the characteristic reflection of clay in the hybrid patterns implies that the layered silicate structure is also preserved. The CNa peak appears almost at the same position in the PTEB/CNa pattern, indicating that the intercalation of PTEB chains within the clay galleries scarcely occurs. The low intensity of the peak suggests some disordering of the clay structure in the hybrid under the solution blending conditions used. In contrast, the C10A peak is shifted from  $4.7^\circ$  to  $2.9^\circ$  in the PTEB/C10A. This effect reflects that

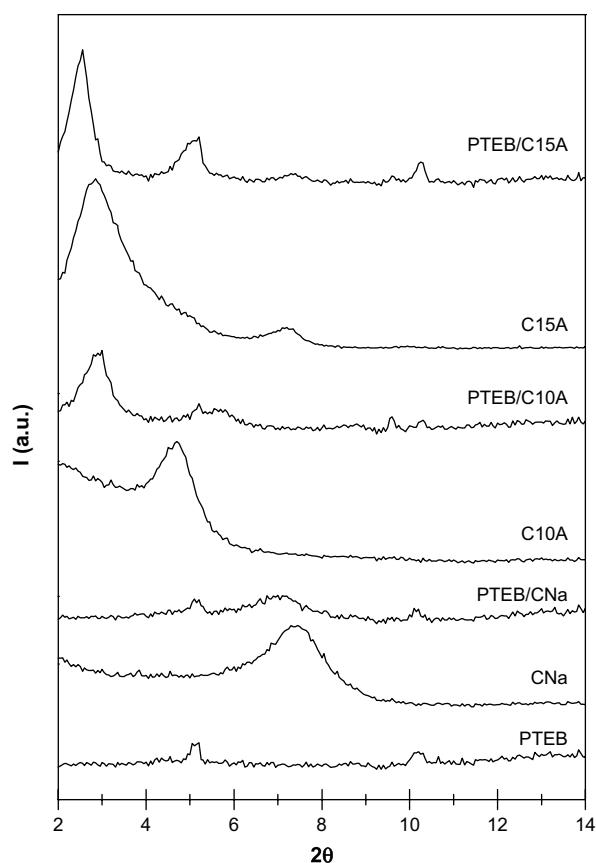


Fig. 1. WAXS patterns at room temperature of the indicated samples. The patterns are shifted vertically for clarity.

the mean interlayer spacing of C10A increases due to the intercalation of polymeric chains, leading to the formation of swollen intercalated structures. Besides, the observation of the second order at around  $5.7^\circ$  is consistent with the formation of a more regular layered silicate structure. The characteristic peak maximum of C15A scarcely changes position in the pattern of PTEB/C15A, but a significant narrowing of the peak is observed. This narrowing implies that a more homogeneous interlayer spacing distribution is attained. The more regular structure of C15A in the hybrid is also manifested by the appearance of the second order of interlayer spacing at  $5.1^\circ$ . The width of the peak is explained by the overlapping with the smectic spacing of PTEB. It can be also observed a weak peak at  $7.4^\circ$ , which may be assigned either to the third order interlayer spacing or to the small silicate population of unmodified montmorillonite retained in C15A.

Fig. 2 displays the TEM images of the hybrids at two magnifications  $\times 10 \text{ K}$  and  $\times 40 \text{ K}$ , giving a general view of the morphology of the PTEB/clay hybrids. The dark spots represent the clay. The micrograph of PTEB/CNa (Fig. 2a and 2d) shows clay aggregates of varying size which are poorly dispersed into matrix. From this result together with the fact that there is scarcely change in the position of the characteristic diffraction peak of clay, it can be concluded that a conventional microcomposite from unmodified montmorillonite is obtained.

In contrast, the micrographs of both PTEB/C10A (Fig. 2b and 2e) and PTEB/C15A (Fig. 2c and 2f) reveal that the clay is well dispersed and exhibits both individual and stacked silicate layers. However, one can observe that PTEB/C15A shows smaller stacks and a higher degree of individual layers. From these observations, together with those made above from X-ray patterns of both hybrids, it can be

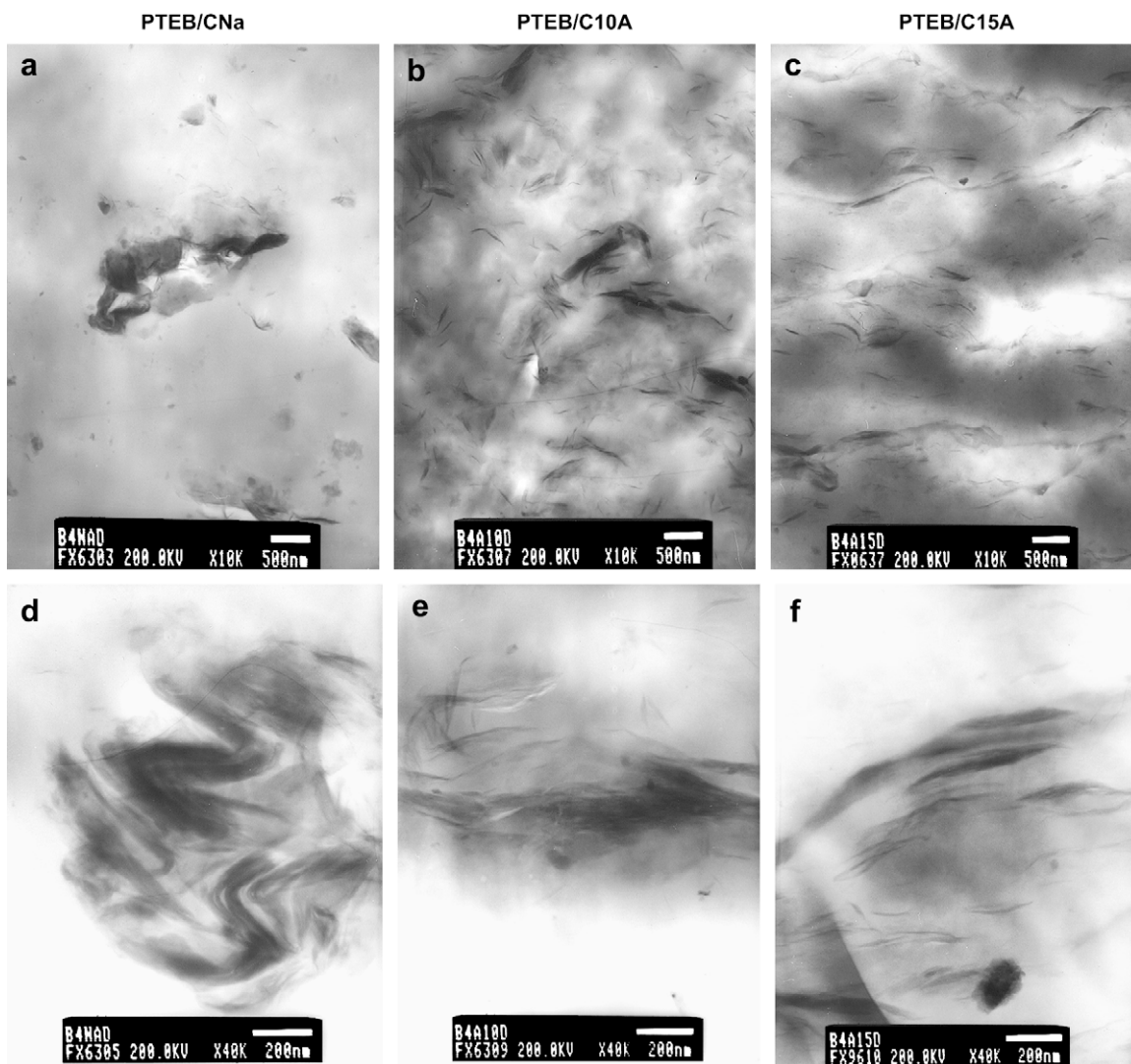


Fig. 2. TEM images of PTEB/clay hybrids. The dark areas represent the clay and the grey/white areas represent the polymer matrix.

concluded that: (1) organic modification of montmorillonite is necessary for the polymer intercalation within the clay gallery, at least under the solution blending conditions used here; (2) the morphology of both PTEB/C10A and PTEB/C15A hybrids is a mixture of intercalated/exfoliated nanostructure, and (3) X-ray data prove that the intercalate stacks of C10A are more swollen by PTEB chains, while TEM micrographs indicate a more exfoliated nanostructure of C15A.

### 3.2. Thermotropic behaviour of PTEB/clay hybrids

PTEB can be quenched into a relatively stable SmC phase from the isotropic melt [14]. The dynamic cooling and heating DSC curves at  $20\text{ }^{\circ}\text{C min}^{-1}$  for neat PTEB and PTEB/clay hybrids are illustrated in Fig. 3. On cooling, PTEB shows the liquid-crystallization exotherm at  $T_{LC} = 101\text{ }^{\circ}\text{C}$ , with an associated enthalpy of  $10.4\text{ J g}^{-1}$ , followed by a glass transition at around  $6\text{ }^{\circ}\text{C}$ . The subsequent heating exhibits again the glass transition, now at  $12\text{ }^{\circ}\text{C}$ , followed by the isotropization endotherm at  $T_i = 116\text{ }^{\circ}\text{C}$ , with an enthalpy of  $10.5\text{ J g}^{-1}$ . The development of the SmC phase in PTEB has been recently studied by variable-temperature synchrotron experiments [17]. We concluded that the exothermic DSC peak detected on cooling from the isotropic melt corresponds to the

formation of a SmA phase, which below  $40\text{ }^{\circ}\text{C}$  is transformed into the tilted SmC mesophase.

A detailed analysis of thermotropic behaviour of PTEB/clay hybrids has been also carried out by DSC and synchrotron experiments. As seen in Fig. 3, only the characteristic PTEB transitions can be detected in the DSC curves of PTEB/clay hybrids, and no important change is observed in the transition temperatures, as well as enthalpy values, of hybrids when compared to those of pure PTEB. The shift of  $T_{LC}$  towards higher temperatures is close to the measurement uncertainty,  $\pm 2\text{ }^{\circ}\text{C}$ . However, the marked narrowing of the peak, together with the slight shift of  $T_{LC}$ , suggests a nucleating effect of clay. This fact will be investigated in detail by isothermal DSC experiments hereinafter.

Fig. 4 presents the MAXS/WAXS profiles simultaneously obtained for PTEB/C10A during the cooling from the isotropic melt at  $8\text{ }^{\circ}\text{C min}^{-1}$ , as an example of the behaviour of the hybrids. The initial pattern, at  $125\text{ }^{\circ}\text{C}$ , shows an amorphous WAXS halo centred at  $2.18\text{ nm}^{-1}$  ( $0.46\text{ nm}$ ) corresponding to the averaged intermolecular distance of PTEB chains in the isotropic melt state, and two MAXS peaks, at  $0.31\text{ nm}^{-1}$  ( $3.22\text{ nm}$ ) and  $0.62\text{ nm}^{-1}$  ( $1.61\text{ nm}$ ), associated with both first and second order of the interlayer spacing of clay. In accordance with the exothermic DSC peak at  $101\text{ }^{\circ}\text{C}$ , the ordering process manifested itself by the appearance of a MAXS

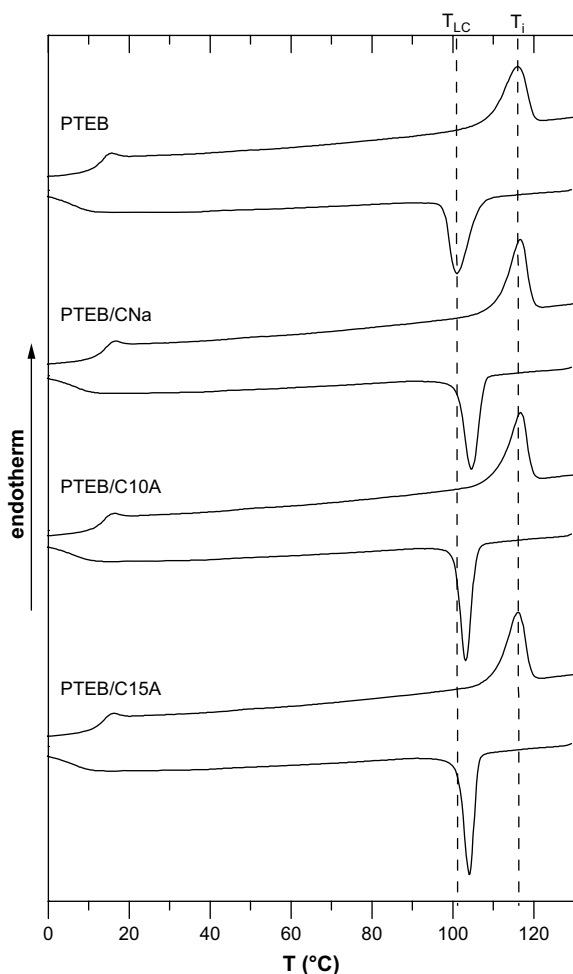


Fig. 3. Cooling-heating DSC curves corresponding to pure PTEB and PTEB/clay hybrids. Scanning rate:  $20\text{ }^{\circ}\text{C min}^{-1}$ .

peak at around  $0.50\text{ nm}^{-1}$  ( $d_{\text{MAXS}} = 2.00\text{ nm}$ ) while a narrowing and a slight change in the maximum position of the WAXS halo is detected. These features indicate the formation of a disordered smectic mesophase. Later on, below around  $50\text{ }^{\circ}\text{C}$ , the layer spacing peak of PTEB shifts to higher  $s$  values (lower spacings), as corresponds to a tilting of the smectic structure.

The temperature dependence on cooling of  $d_{\text{MAXS}}$  for PTEB/CNa and PTEB/C10A hybrids is shown in Fig. 5. Unfortunately, the overlapping of the smectic peak with the second order of the clay peak prevents the corresponding analysis in the case of PTEB/C15A. Previous reported data for neat PTEB are also represented. It can be observed a similar temperature dependence of  $d_{\text{MAXS}}$  for hybrids and neat PTEB. In short, from the appearance of the smectic peak down to about  $47\text{ }^{\circ}\text{C}$ , the value of spacing is close to the length of the extended repeating unit of PTEB [14] indicating that a SmA phase is formed first; below  $47\text{ }^{\circ}\text{C}$ , the spacing begins to decrease with temperature due to the tilting of molecules respect to the smectic plane, leading to a SmC phase. Therefore, it can be concluded that the cooling phase sequence (isotropic melt-SmA-SmC) is practically unaffected by the presence of clay particles. In contrast, the kinetics of the phase transformations is clearly affected, as shown below. Regarding the smectic layer thickness, although the differences are almost inside the experimental error, it seems that slightly greater layer spacings are obtained in the hybrids.

### 3.3. Effect of clay on liquid-crystallization and crystallization of PTEB/clay hybrids

The effect of clay on the formation of the SmA phase in PTEB has been examined by isothermal DSC measurements. The heat flow curves of PTEB and PTEB/clay hybrids during isothermal liquid-crystallization, in the temperature range  $T = 112\text{--}106\text{ }^{\circ}\text{C}$ , have been registered in the DSC. The kinetics of liquid-crystallization may be better visualized by plotting fractional liquid-crystallization,  $X_{\text{LC}}$ , vs. time.

For the purpose of comparison, the curves obtained at  $108\text{ }^{\circ}\text{C}$  for pure PTEB and PTEB/clay hybrids are compiled together and shown in Fig. 6. One can observe that the transformation is rather fast in all the samples. However, the onset time of liquid-crystallization occurs at significantly shorter times for PTEB/clay hybrids. Moreover, they display a stronger upswing in the fractional liquid crystallinity, reaching unity after around 0.6 min, whereas 1.6 min is needed for the complete transformation of neat PTEB.

The liquid-crystallization rate can be expressed in terms of the liquid-crystallization half time,  $t_{1/2}$ , the time necessary to reach the 50% of isotropic melt-liquid-crystalline conversion. Fig. 7a shows  $t_{1/2}$  values for pure PTEB and PTEB/clay hybrids as a function of temperature in terms of undercooling  $\Delta T = T_i - T$ . From our dynamic DSC results we assume that  $T_i$  is  $116\text{ }^{\circ}\text{C}$  for all the samples studied. It is apparent that  $t_{1/2}$  increases for all samples assumingly exponentially with decreasing undercooling, at least within the temperature range studied. Moreover, it can be observed that PTEB/clay hybrids have shorter  $t_{1/2}$  than neat PTEB in the whole experimental temperature range, indicating faster liquid-crystallization rate. In fact, for undercooling values higher than  $8\text{ }^{\circ}\text{C}$ , the formation of the SmA mesophase in the hybrids is too rapid for studying it by DSC.

To obtain more insightful information about the mechanism of SmA formation in the PTEB/clay hybrids, a simplified Avrami analysis was also used to analyse the isothermal liquid-crystallization kinetics. The Avrami approximation [19] is often used to describe the initial stage of crystalline order in polymers according to the equation:

$$1 - X(t) = \exp(-kt^n) \quad (1)$$

where  $X(t)$  is fraction of crystallized material at time  $t$ ,  $k$  is the temperature-dependent rate constant and  $n$  the Avrami exponent. Both  $k$  and  $n$  are specific constants for a given crystalline morphology and type nucleation and for a particular crystallization condition [20]. The Avrami exponent  $n$  is normally an integer, ranging from 1 to 4. The values of  $n$  and  $k$  can be obtained from the slope and intercept, respectively, of the double-logarithmic plot,  $\ln[1 - \ln(1 - X(t))]$  against  $\ln t$ . Eq. (1) has been also reported for the kinetics of isotropic-mesomorphic transitions. Considerably different values of  $n$ , from 1 to about 4 have been found, indicating that the liquid-crystallization kinetics of polymers is further influenced by the liquid-crystalline order. So, exponent  $n$  approximates 1 for nematics [21], and values within 2–4 for smectics [22] were found.

The analysis of experimental data for PTEB and PTEB/clay hybrids shows a good adherence to Eq. (1) for only the early stages of the liquid-crystallization process. The Avrami equation is not applicable in the late stages, where slower processes take place. The Avrami parameters for neat PTEB and PTEB/clay hybrids fitted to the experimental data at  $X(t) < 0.5$  are given in Fig. 7b and c as function of undercooling. It can be observed that neat PTEB and hybrids present values of  $n$  between 2 and 3 in the undercooling range measured. These values are consistent with two or three-dimensional growth of the SmA phase following homogeneous/heterogeneous nucleation. One can see that the value of  $n$  for neat

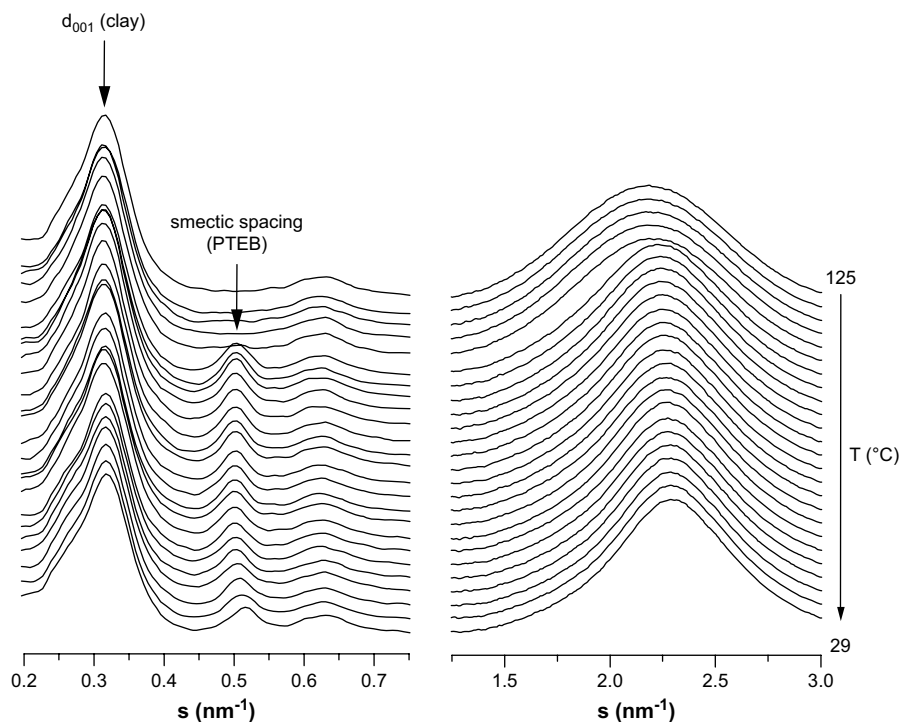


Fig. 4. Simultaneous MAXS (left side) and WAXS (right side) X-ray patterns during the cooling from the isotropic melt, at  $8\text{ °C min}^{-1}$ , of PTEB/C10A hybrid. The different patterns are shown every  $4\text{ °C}$ .

PTEB varies around an average of 2.8 and  $k$  decreases about two orders the magnitude in a temperature range of  $5\text{ °C}$ . The Avrami parameters for PTEB/CNa sample show clearly an analogous behaviour to that of neat PTEB. In contrast, the exponent  $n$  for both PTEB/C10A and PTEB/C15A samples shows a tendency to decrease at lower undercoolings. Moreover, the overall rate constant,  $k$ , is not very much dependent on  $T$  in the experimental temperature range.

So far, it can be concluded that the clay particles act as nucleating agent for the SmA phase of PTEB. Furthermore, the Avrami analysis seems to suggest that there is some influence of the clay morphology on the kinetics of liquid crystallization. The decrease of the Avrami exponent  $n$  in both PTEB/C10A and PTEB/C15A could be ascribed to a hindering of the liquid-crystalline order growth due to the confinement of polymer chains between silicate layers.

Important effects of the clay can be also expected in the crystallization of PTEB since three-dimensional ordering is involved. With this idea in mind, the isothermal crystallization from the mesophase of PTEB/clay hybrids has been investigated.

The transformation of the mesophase of PTEB into a three dimensional crystal can be attained by annealing at temperatures above the glass transition for a long time [15,16]. Fig. 8a shows the DSC heating curves for PTEB samples after thermal treatment at  $85\text{ °C}$ . It can be observed that the annealed samples show an additional endotherm at  $102\text{ °C}$  whose intensity increases as annealing time increases. Variable-temperature X-ray diffraction experiments [23] have confirmed that this endotherm corresponds to a crystal-SmA transformation.

PTEB/clay hybrids were also annealed at  $85\text{ °C}$ . As an example, Fig. 8b illustrates the DSC heating curves obtained for PTEB/C10A. A similar behaviour to that of PTEB is observed: the crystal-SmA transition at  $102\text{ °C}$  and the mesophase isotropization at  $116\text{ °C}$ . Fig. 9 shows the variation with annealing time of the melting enthalpy,  $\Delta H_m$ , of the peak at  $102\text{ °C}$  for PTEB and PTEB/clay hybrids. It is observed that for all the samples the enthalpy increases up to an asymptotic value of around  $21.0\text{ J g}^{-1}$ . This means

that the same degree of crystallization is reached. The curves of neat PTEB and PTEB/CNa microcomposite can be considered similar within the experimental error. The most different behaviour is found in the PTEB/C10A hybrid, where the crystallization induction

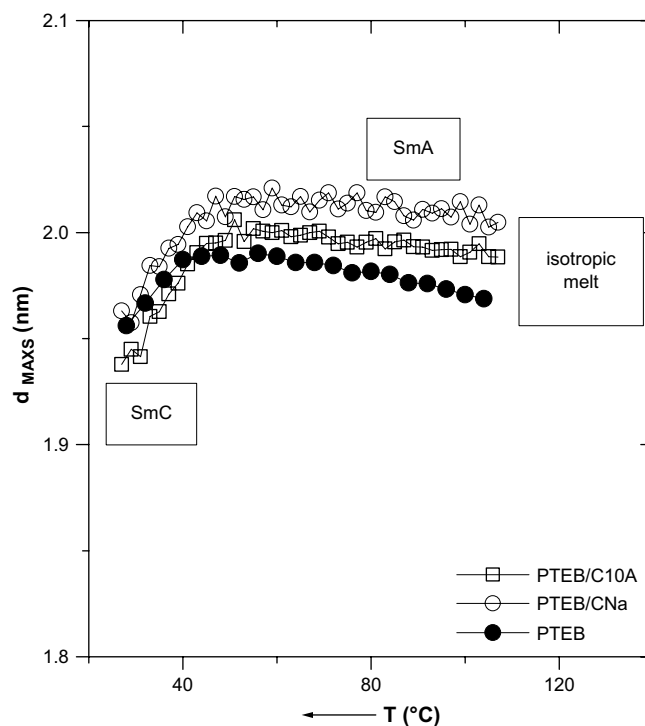


Fig. 5. Variation with temperature of the position of the smectic spacing corresponding to PTEB/C10A and PTEB/CNa hybrids during the cooling from the isotropic melt. Data reported for neat PTEB are also represented, for comparison.

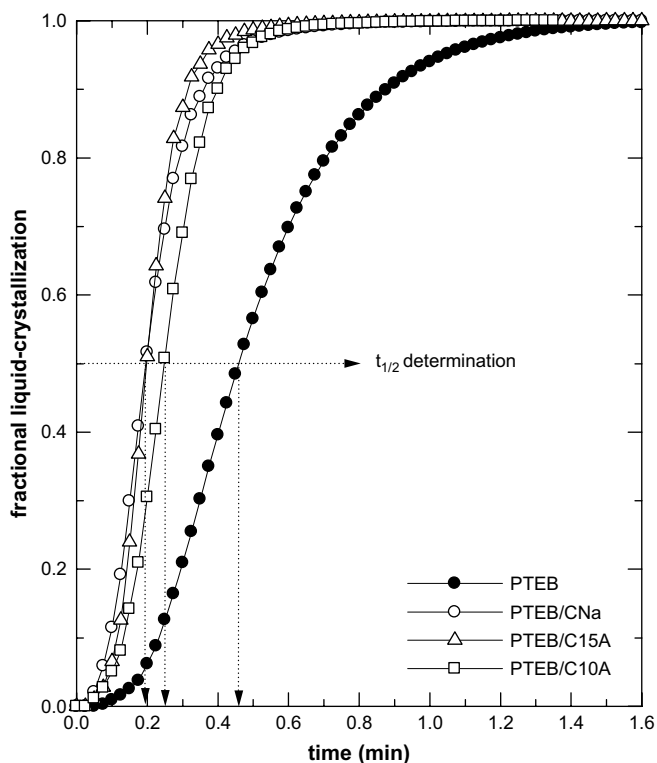


Fig. 6. Fractional liquid-crystallization curves as a function of time during isothermal experiment at 108 °C for the different samples.

period and the crystallization half time increase by a factor of two. An intermediate behaviour is found for the hybrid PTEB/C15A.

Therefore, it is evident that the microstructure of CNa has no effect on the crystallization of PTEB while the intercalated/exfoliated nanostructure of C10A and C15A retards it. However, a higher retardation of crystallization is produced in PTEB/C10A. Xu et al. [24] have studied the isothermal crystallization kinetics of two samples of polyethylene/montmorillonite nanocomposite with different dispersion states of clay. They have observed that the intercalated sample has longer induction period and longer crystallization half time than the exfoliated sample. This behaviour has been mainly attributed to the confinement effect of the MMT layers. Based on this study, the slower crystallization rate found in PTEB/C10A could be ascribed to the higher confinement of polymer chains within the galleries of C10A, reducing the chain mobility. This fact is consistent with the higher swelling of C10A observed by X-ray. Moreover, the interaction of benzyl moieties of the surfactant with the polymer matrix should further reduce the mobility of polymer chains.

### 3.4. Tensile properties

The stress–strain curves of the PTEB and PTEB/clay hybrids are shown in Fig. 10. Neat PTEB shows a marked yield strength, which is related to the development of the neck, followed by cold drawing and strain hardening [6]. One can observe that the introduction of clay into the PTEB matrix produces an increase in the yield strength, indicating that the plastic deformation in the hybrids starts at a higher stress than neat PTEB. Fig. 11 represents Young's modulus and yield strength for all the samples. It is observed that the unmodified sodium montmorillonite leads to a smaller improvement in tensile properties than organoclays do. Increases of about

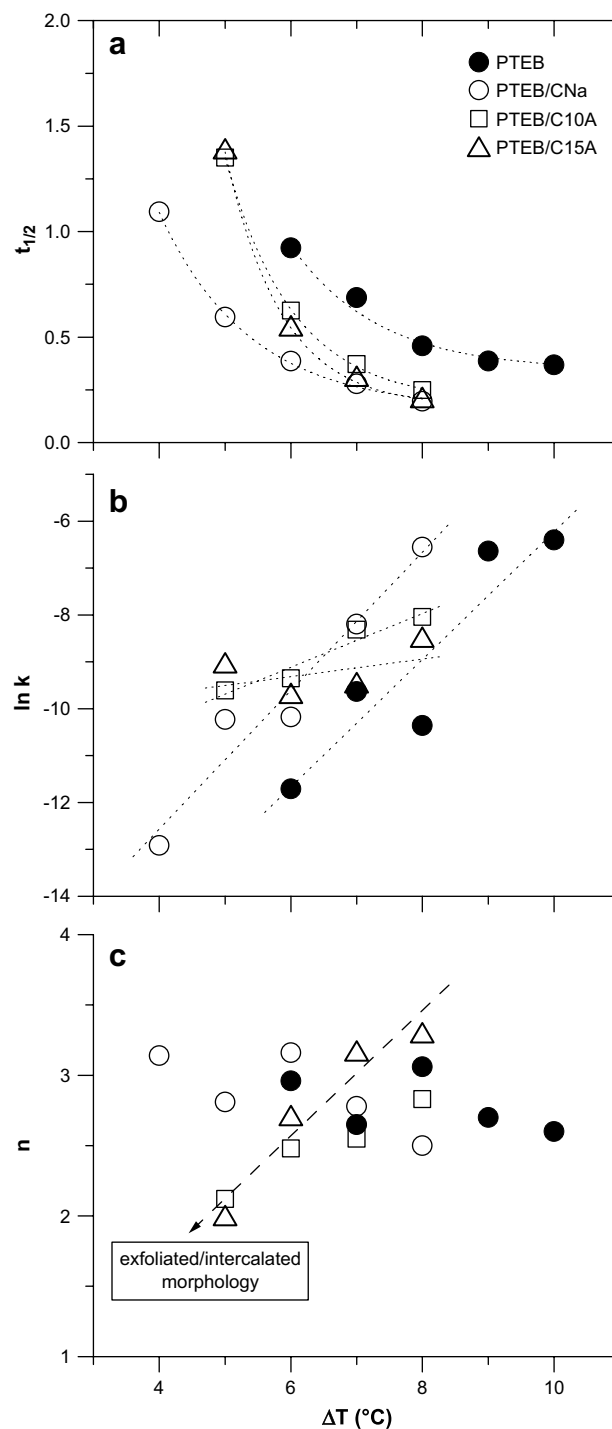


Fig. 7. Variation with temperature of (a) half-times of isothermal liquid-crystallization and of (b and c) Avrami parameters, for PTEB and PTEB/clay hybrids. Data are represented in terms of undercooling,  $\Delta T = T_i - T$ .

200% and 50% of Young's modulus and yield strength, respectively, have been found for both PTEB/C15A and PTEB/C10A. It is widely accepted that the improvement in tensile properties, modulus and strength, depends on the clay–polymer interactions. Thus, the increase can be attributed to the intercalated/exfoliated morphology, which gives rise to a larger interface compared to that achieved in the PTEB/CNa microcomposite.

Fig. 10 also shows that elongation at break is smaller in all hybrids. Tensile strength at break in PTEB/CNa microcomposite is

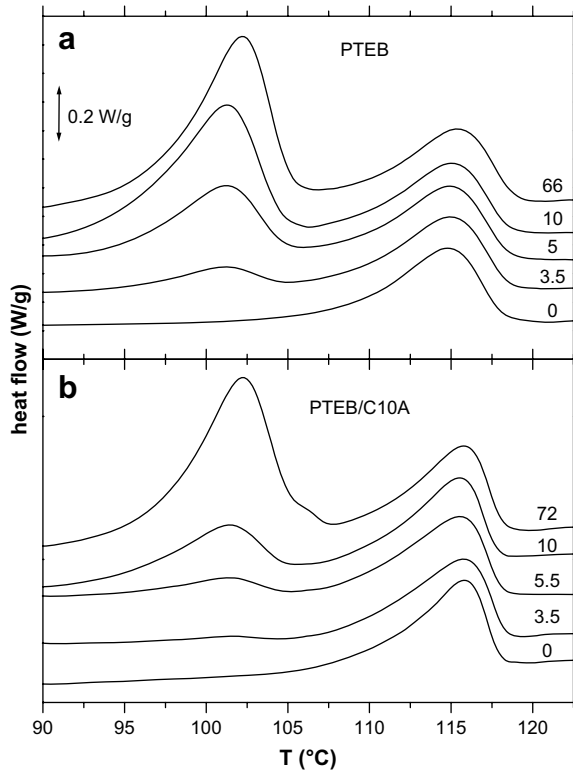


Fig. 8. DSC heating curves, recorded at 10 °C min<sup>-1</sup>, after annealing (a) neat PTEB and (b) PTEB/C10A hybrid at 85 °C for the indicated annealing times (in hours). The curves are shifted vertically for clarity.

higher than yield strength due to a strong strain hardening before break. PTEB/C15A sample exhibits a degree of unbonding following the peak stress, whereas PTEB/C10A sample fails in a more brittle manner once the yield point is exceeded. From these results, it is

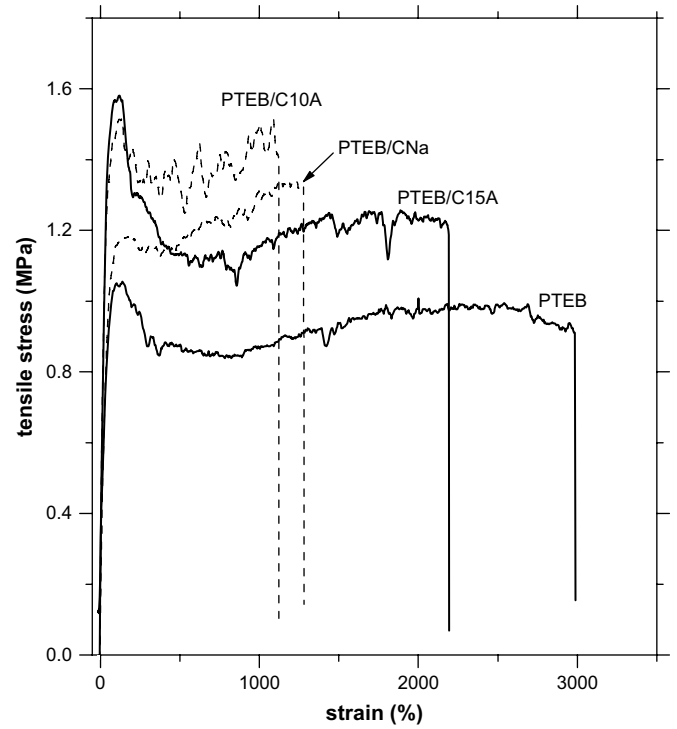


Fig. 10. Stress–strain curves of PTEB and PTEB/clay hybrids.

evident that the nanostructure of clay in the hybrids affects the elongation at break of PTEB. The lower ductility in the PTEB/C10A is consistent with the higher reduction of mobility of polymer chains.

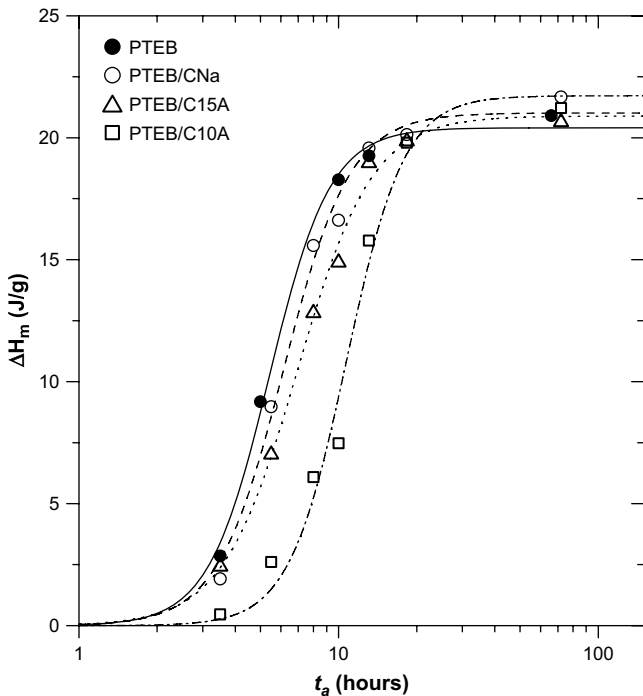


Fig. 9. Variation with annealing time,  $t_a$ , of the melting enthalpy,  $\Delta H_m$ , for PTEB and PTEB/clay hybrids annealed at 85 °C. Lines represent the sigmoidal fit of data.

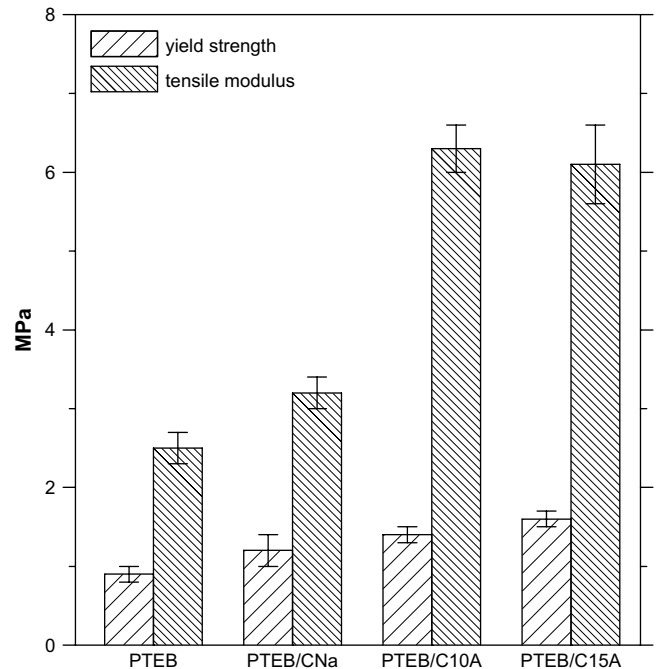


Fig. 11. Yield strength and Young's modulus of PTEB and PTEB/clay hybrids.



#### 4. Conclusions

PTEB/layered silicate nanocomposites have been obtained from organically modified montmorillonite via solution blending procedure. Both C10A and C15A clays lead to a morphology which can be considered as a mixture of intercalated/exfoliated nanostructure. Furthermore, X-ray diffractograms prove that C10A leads to highly swollen intercalated stacks, while TEM micrographs show that C15A exhibits a higher degree of individual layers. In contrast, a conventional microcomposite has been attained from the unmodified montmorillonite (CNa). Therefore, the exfoliation degree attained depends on both the nanostructure of neat clay and the chemistry of the surfactant.

DSC and synchrotron experiments indicate that the liquid-crystalline character of PTEB is preserved in the hybrids, and both the cooling phase sequence (isotropic melt–SmA–SmC) and smectic layer thickness of PTEB are practically unaffected by the presence of clay particles.

The kinetics of the isotropic–SmA transformation of PTEB is faster in all hybrids. On the one hand, the lower value of  $t_{1/2}$  in the hybrids indicates that the clay particles act as nucleating agent for the SmA phase of PTEB. On the other hand, the decrease of the Avrami exponent in both PTEB/C10A and PTEB/C15A could be ascribed to a hindering of the liquid-crystalline order growth, due to the confinement of polymer chains between silicate layers. The confinement effect of chains is clearly predominant during the isothermal transformation of the smectic mesophase of PTEB into a three dimensional crystal. The two nanocomposites show a retardation of crystallization of PTEB matrix. However, PTEB/C10A has a slower crystallization rate than PTEB/C15A. Thus, it seems that the more swollen nanostructure of PTEB/C10A leads to a higher reduction of mobility of PTEB chains.

The tensile behaviour is clearly influenced by the morphology of the hybrids. The microcomposite morphology of PTEB/CNa leads to a smaller improvement in yield strength and Young's modulus than the nanocomposite morphology of PTEB/C10A and PTEB/C15A. Both nanostructured hybrids show an increase of Young's modulus of about 200% with respect to neat PTEB. However, PTEB/C10A has poorer ductility than PTEB/C15A. This fact is consistent with the higher reduction of mobility of polymer chains in PTEB/C10A.

#### Acknowledgements

We acknowledge the financial support of MICIIN, Projects MAT2007-65519-C02-02 and MAT2007-65519-C02-01. The synchrotron work was supported by the European Community-Research Infrastructure Action under the FP6 'Structuring the European Research Area' Programme through the Integrated Infrastructure Initiative, 'Integrating Activity on Synchrotron and Free Electron Laser Science', contract RII3-CT-2004-506008. We thank the collaboration of the HasyLab personnel.

#### References

- [1] Chiellini E, Laus M. In: Demus D, Goodby J, Gray GW, Spiess HW, Vill V, editors. Handbook of liquid crystals, vol. 3. Weinheim: Wiley-VCH; 1998.
- [2] Tjong SC. *Mat Sci Eng R* 2006;53(3–4):73–197.
- [3] Vaia RA, Giannelis EP. *Polymer* 2001;42(3):1281–5.
- [4] Chang J-H, Seo B-S, Hwang D-H. *Polymer* 2002;43(10):2969–74.
- [5] Huang W, Han CD. *Polymer* 2006;47(12):4400–10.
- [6] Pérez E, Pereña JM, Benavente R, Bello A. In: Cheremisinoff NP, editor. Handbook of engineering polymeric materials. New York: Marcel Dekker; 1997. p. 383–97.
- [7] Pérez E, del Campo A, Bello A, Benavente R. *Macromolecules* 2000;33(8):3023–30.
- [8] Bello P, Bello A, Riande E, Heaton NJ. *Macromolecules* 2001;34(2):181–6.
- [9] Martínez-Gómez A, Bello A, Pérez E. *Macromolecules* 2004;37(23):8634–40.
- [10] Martínez-Gómez A, Bello A, Pérez E. *e-Polymers* 2008;69:1–16.
- [11] Martínez-Gómez A, Pereña JM, Lorenzo V, Bello A, Pérez E. *Macromolecules* 2003;36(15):5798–803.
- [12] Fernández-Blázquez JP, Bello A, Pérez E. *Macromol Chem Phys* 2007;208(24):2611–20.
- [13] Nguyen QT, Baird DG. *Adv Polym Technol* 2006;25(4):270–85.
- [14] Pérez E, Riande E, Bello A, Benavente R, Pereña JM. *Macromolecules* 1992;25(2):605–10.
- [15] Benavente R, Pereña JM, Pérez E, Bello A, Lorenzo V. *Polymer* 1994;35(17):3686–90.
- [16] Pérez E, Benavente R, Bello A, Pereña JM, Vanderhart DL. *Macromolecules* 1995;28(18):6211–8.
- [17] Álvarez C, Martínez-Gómez A, Pérez E, de la Orden MU, Martínez Urreaga J. *Polymer* 2007;48(11):3137–47.
- [18] Data Sheet. Texas: Shouthern Clay Product Inc.
- [19] Avrami M. *J Chem Phys* 1939;7(12):1103–12; *J Chem Phys* 1940;8(2):212–24; *J Chem Phys* 1941;9(2):177–84.
- [20] Wunderlich B. *Macromolecular physics: crystal nucleation, growth, annealing*, vol. 2. New York: Academic Press; 1976.
- [21] Liu SL, Chung TS, Lu L, Torii Y, Oikawa H, Yamaguchi A. *J Polym Sci Part B Polym Phys* 1998;36(10):1679–94.
- [22] Tsai R-S, Tsai H-B, Hu A-T, Lee Y-D. *Makromol Chem* 1992;193(9):2477–86.
- [23] Pérez E, Martínez-Gómez A, Fernández-Blázquez JP, Rodríguez-Amor V, Bello A, Cerrada ML, et al. HASYLAB annual report; 2007. pp. 1429–1430.
- [24] Xu J-T, Zhao Y-Q, Wang Q, Fan Z-Q. *Polymer* 2005;46(25):11978–85.